Engineering Structures 175 (2018) 355–370

Contents lists available at ScienceDirect

Engineering Structures

journal homepage: www.elsevier.com/locate/engstruct

Experimental and numerical study of stainless steel I-sections under concentrated internal one-flange and internal two-flange loading

G.B. dos Santos[a,*], L. Gardner[a], M. Kucukler[a,b]

[a] Department of Civil and Environmental Engineering, South Kensington Campus, Imperial College London, London SW7 2AZ, UK
[b] Department of Civil Engineering, Bilecik Seyh Edebali University, Bilecik 11210, Turkey

ARTICLE INFO

Keywords:
Austenitic stainless steel
Concentrated transverse load
Experiments
Finite element modelling
Internal one-flange (IOF)
Internal two-flange (ITF)
Testing

ABSTRACT

The behaviour and design of stainless steel I-section beams under concentrated transverse loading are investigated in this study. Twenty-four experiments on stainless steel I-sections, formed by the welding of hot-rolled plates, were performed. The tests were conducted under two types of concentrated transverse loading – internal one-flange (IOF) and internal two-flange (ITF) loading. The experimental set-up, procedure and results, including the full load-displacement histories, ultimate loads and failure modes, are reported. A complementary nonlinear finite element modelling study was also carried out. The models were first validated against the results of the experiments. A parametric investigation into the influence of key parameters such as the bearing length, web slenderness and level of coexistent bending moment, on the structural response was then performed. Finally, an assessment of current design provisions for the resistance of stainless steel welded I-sections to concentrated loading is presented. The results show that the current design formulae yield safe-sided, but generally rather scattered and conservative capacity predictions, with considerable scope for further development.

1. Introduction

Structural steel members under concentrated transverse loading are encountered in a wide range of situations – examples include primary girders at bearing supports, primary beams under roof purlins, columns in beam-to-column connections [1] and bridge girders during their launching phase [2,3]. Members under concentrated transverse loading are subjected to non-uniform stress distributions, complex edge restraint conditions between the web and flanges, and local yielding beneath the load [4]. Taken together, these render the development of analytical formulations able to predict accurately the ultimate resistances of members under concentrated loading non-trivial. Even analytical models for the key reference points of the elastic buckling load and plastic collapse load [5,6], which can be used to predict ultimate resistance, are still complex, and numerical techniques are often necessary for their accurate determination [7,8].

Experimental investigations carried out to determine the ultimate bearing resistances of steel members under concentrated transverse loading date back to 1946, when the first tests on cold-formed carbon steel members were reported by Winter and Pian [9]. Such tests have since been performed on cold-formed carbon steel members with different cross-section shapes, including I-sections, C-sections, Z-sections, hat-sections, deck sections, and hollow sections [10–14], on members with and without flange restraints [15–18], and web openings [19–21], and on cold-formed stainless steel members [22–25]. Numerical studies on cold-formed stainless steel members have also been performed [23,26–28]. Tests on cold-formed members are often referred to as *web crippling tests* due to the failure mode exhibited during the experiments. A substantial number of tests has also been carried out on hot-rolled and welded I-section members with slender [29,30] and stocky webs [31], considering different bearing lengths [32–34] coincident bending moments [35,36] and including sections made of high strength steel [37]. There exist, however, very few tests on welded stainless steel I-section members subjected to concentrated transverse loading [38].

The structural performance of stainless steel members under concentrated transverse loading is the focus of the present study. Two types of concentrated transverse loading are considered: (i) internal one-flange loading resulting in failure beneath a single concentrated load away from the beam end, and (ii) internal two-flange (ITF) loading, leading to failure between two concentrated loads applied at opposite flanges away from the beam end. An experimental investigation involving twenty-four physical tests to

* Corresponding author.
E-mail address: g.santos14@imperial.ac.uk (G.B. dos Santos).

https://doi.org/10.1016/j.engstruct.2018.08.015
Received 16 April 2018; Received in revised form 24 July 2018; Accepted 8 August 2018
Available online 22 August 2018

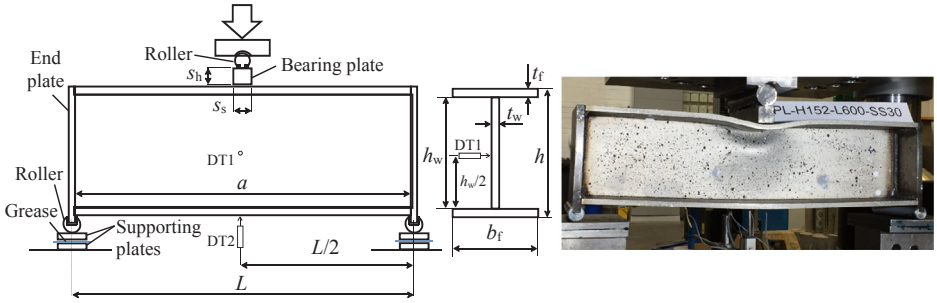

(a) Schematic setup (b) Test setup

Fig. 1. Experimental setup for IOF specimens.

examine the influence of different bearing lengths and bending moments on the ultimate resistance of stainless steel beams under IOF and ITF loading is first presented. Following this, numerical models, validated against the results of the physical experiments, are used to generate further data across a broad range of practical cases. Finally, the experimental and numerical results are employed to assess the accuracy of existing design provisions [39,40] for the design of stainless steel members under concentrated transverse loading.

2. Experimental investigation

Sixteen internal one-flange (IOF) loading tests and eight internal two-flange (ITF) loading tests were carried out to assess the web bearing strengths of stainless steel I-section members. The specimens were fabricated from hot-rolled stainless steel plates which were laser-welded in accordance with EN ISO 13919-1 [41]; the quality level was Class B (stringent). Four cross-section sizes were examined: (i) I 102 × 68 × 5 × 5, (ii) I 152 × 160 × 6 × 9, (iii) I 150 × 75 × 7 × 10, and (iv) I 160 × 82 × 10 × 12. The cross-sections were formed from austenitic stainless steel of different grades: Grade EN 1.4571 for the first two cross-sections, Grade EN 1.4404 for the third and Grade EN 1.4307 for the fourth. The IOF tests, the setup for which is shown in Fig. 1, were performed on three different cross-section sizes with different bearing lengths and a range of spans, while the ITF tests, the setup for which is depicted in Fig. 2, were carried out on two different cross-section sizes with different bearing lengths. Both test series were designed to cover a range of structural responses and isolate the influence of the key parameters. The adopted test labelling system identifies the loading type (IOF or ITF), and the nominal cross-section height (102 mm, 150 mm, 152 mm, or 160 mm), specimen length (from 300 mm to 750 mm) and bearing length s_s (from 5 mm to 100 mm); for example, IOF-H102-L500-SS20 indicates a member under IOF loading with a cross-section height of 102 mm, a length of 500 mm and a bearing length of 20 mm. In the following subsections, the member tests, together with the accompanying material coupon tests and geometric imperfection measurements, are reported.

2.1. Material testing

A comprehensive characterization of the tensile stress-strain properties of the cross-sections tested herein can be found in Gardner et al. [42]; in this section, a brief summary is provided. All the tensile coupon tests were performed according to EN ISO 6892-1 [43], using an Instron 8802 250 kN hydraulic testing machine. The coupons were extracted from the longitudinal direction of the members. For cross-sections comprising plates of the same thickness, a single coupon test was performed, while for those fabricated from plates of different thicknesses, two coupon tests (one from the web and one from the flanges) were carried out. A summary of the measured tensile material properties for each cross-section size is given in Table 1, where E is the Young's modulus, f_y is the 0.2% proof stress, $f_{1.0}$ is the 1% proof stress, f_u is the ultimate tensile stress, ε_u is the strain the at ultimate stress, and ε_f is the strain at the fracture, measured over the standard gauge length.

2.2. Geometric dimensions and imperfection measurements

Prior to the member tests, the dimensions and geometric imperfections of the specimens were measured. The initial imperfection measurements were taken using the setup shown in Fig. 3, following a similar procedure to that employed by Schafer and Pekoz [44] and Zhao et al. [45]. A Linear Variable Displacement Transducer (LVDT) was attached to the head of a milling machine, while the specimens were secured to the moving machine bed. The LVDT was utilised to measure the variation in the out-of-plane

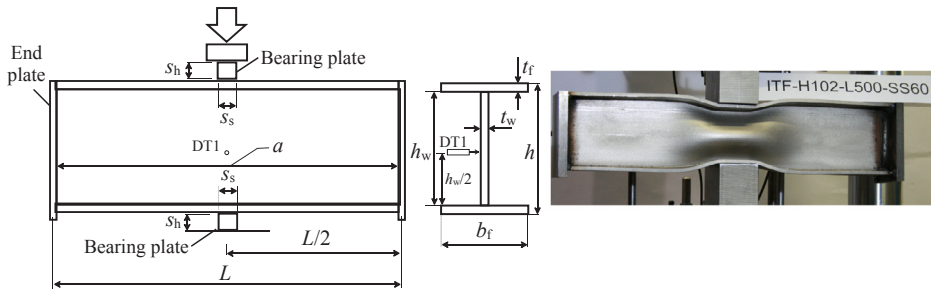

(a) Schematic setup (b) Test setup

Fig. 2. Experimental setup for ITF specimens.

Table 1
Summary of material properties measured from tensile coupon tests [42].

Specimen	E (N/mm^2)	f_y (N/mm^2)	$f_{1.0}$ (N/mm^2)	f_u (N/mm^2)	ε_u (%)	ε_f (%)
I 102 × 68 × 5 × 5	186,800	222	331	580	50	64
I 150 × 75 × 7 × 10 (Web)	197,300	274	344	596	58	68
I 150 × 75 × 7 × 10 (Flange)	197,200	267	323	560	50	66
I 152 × 160 × 6 × 9 (Web)	191,400	272	349	586	50	65
I 152 × 160 × 6 × 9 (Flange)	204,700	227	287	561	52	67
I 160 × 82 × 10 × 12 (Web)	198,500	264	341	618	53	64
I 160 × 82 × 10 × 12 (Flange)	197,500	286	342	619	52	65

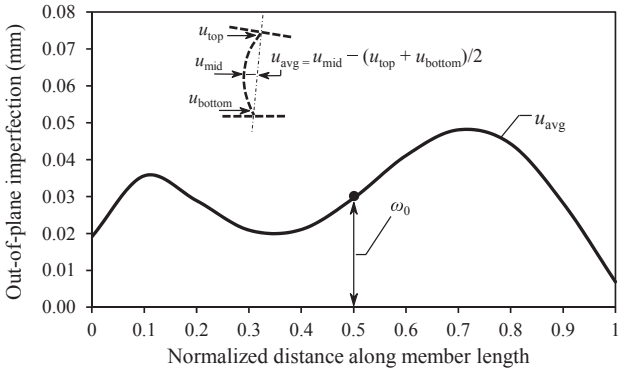

Fig. 4. Measured out-of-plane geometric imperfections u_{avg} for IOF-H102-L300-SS10 test specimen.

displacement along the top, mid-height and bottom lines across the web length of the specimens. To eliminate the influence of the weld geometry, the measurements were taken 10 mm away from the web-to-flange junctions, as shown in Fig. 3(a). The local web imperfection amplitude ω_0 for each specimen was taken as the difference between the mid-height (u_{mid}) displacement reading and the average of the displacement readings along the top (u_{top}) and bottom (u_{bottom}) of the web, under the concentrated load (i.e. at mid-span) as shown in Fig. 4. The measured dimensions and geometric imperfections of the IOF and ITF test specimens are reported in Tables 2 and 3, respectively, where h is the cross-section depth, t_w is the web thickness, b_f is the flange width, t_f is the flange thickness, s_s is the bearing length (equal to the bearing height s_h), L is the beam span, h_{ep}, $b_{f,ep}$ and t_{ep} are the end plate height, width and thickness respectively, and ω_0 is the measured web imperfection under the concentrated load.

2.3. Internal one-flange loading tests

The internal one-flange (IOF) test setup consisted of a three-point bending configuration with the load applied through a bearing plate at mid-span, as shown in Fig. 1. Two carbon steel plates were welded to the ends of the specimens and supported on rollers, which were configured to slide horizontally in response to the applied loading. The bearing plate, through which the loading was applied, had a roller welded to the top, which allowed rotation about the out-of-plane axis, but no horizontal translation. Displacement control was adopted in the tests driving an Instron 8800 750 kN hydraulic testing machine at a constant rate of 0.005 mm/s. Displacement transducers (DTs) were used to capture the out-of-plane web displacement (DT1) and the vertical displacement at the bottom flange (DT2) of the beams. The vertical displacement of the machine was also recorded. Fig. 5 shows the failed specimens, all of which exhibited out-of-plane deformation of the web beneath the applied load and flange bending. The load-vertical displacement responses of the IOF test specimens are provided in Figs. 6–8, the load-web shortening responses are provided in Figs. 9–11 and the load versus web out-of-plane displacement responses are shown in Figs. 12–14. The vertical web shortening was determined by taking the difference between the vertical displacement of the testing machine and the vertical displacement measured at the bottom flange of the specimen (DT2). The key IOF test results are presented in Table 2, where F_u is the ultimate test load, δ_u is the vertical web shortening at the ultimate load and $\delta_{u,v}$ is the vertical displacement of the top flange at the ultimate load.

The out-of-plane deformation field of the webs of the tested members was also recorded using a Digital Image Correlation (DIC) system. A random speckle pattern was first applied to the web surface of each of the tested specimens. Two high-resolution cameras were used to monitor the web region during the tests. Images were taken at 3 s intervals and were processed using the software DaVis 8.4.0 [46]. Fig. 15 shows the load-out-of-plane displacement response, together with the out-of-plane deformation fields obtained from the DIC data at different stages during the testing of specimen IOF-H150-L400-SS60. The out-of-plane deformation fields indicate that the maximum out-of-plane displacement occurred at mid-span under the point of load application above the mid-height of the web.

2.4. Internal two-flange loading tests

The internal two-flange (ITF) test setup shown in Fig. 2 consists of a member subjected to two simultaneous transverse loads applied through two bearing plates, one positioned at the top flange and the other at the bottom flange. Both bearing plates had the same dimensions and were placed at the mid-span of the member. Carbon steel plates were welded to both ends of the test specimens. Similar to the IOF tests, the ITF tests were performed under displacement control at a constant rate of 0.005 mm/s using an

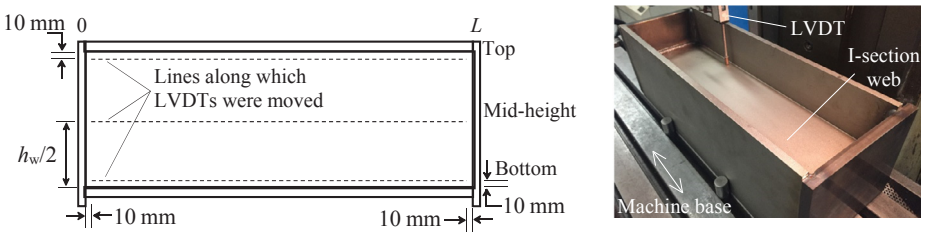

(a) Schematic setup (b) Test setup

Fig. 3. Imperfection measurement setup.

Table 2
Summary of measured dimensions, geometric imperfections and test results of the IOF specimens.

Specimen	h (mm)	t_w (mm)	b_f (mm)	t_f (mm)	$s_s = s_h$ (mm)	L (mm)	a (mm)	h_{ep} (mm)	$b_{f,ep}$ (mm)	t_{ep} (mm)	ω_0 (mm)	F_u (kN)	δ_u (mm)	$\delta_{u,v}$ (mm)
IOF-H150-L150-SS60	149.9	6.95	75.8	9.91	60.0	162.0	149.9	161.3	89.9	12.1	0.098	424.4	6.2	7.1
IOF-H150-L200-SS60	150.0	6.87	75.8	9.79	60.0	212.2	200.1	161.4	89.8	12.1	0.056	393.1	3.4	5.1
IOF-H150-L300-SS60	149.9	6.88	75.8	9.76	60.0	313.1	301.0	162.1	89.9	12.1	0.055	368.6	3.2	6.5
IOF-H150-L400-SS60	150.2	6.81	75.7	9.80	60.0	414.1	402.0	161.6	89.9	12.1	0.029	342.2	9.2	6.8
IOF-H150-L450-SS60	150.0	6.87	75.7	9.79	60.0	464.1	452.0	161.7	89.9	12.1	0.041	340.0	9.9	7.8
IOF-H152-L150-SS30	151.7	6.20	160.0	8.73	30.0	162.2	150.0	164.5	150.0	12.2	0.007	340.0	6.2	6.7
IOF-H152-L300-SS30	152.9	6.18	159.0	8.77	30.0	313.1	301.0	164.0	150.1	12.1	0.058	322.2	4.6	6.5
IOF-H152-L450-SS30	152.0	6.22	159.6	8.73	30.0	463.1	451.0	164.3	150.1	12.1	0.017	301.1	3.8	6.3
IOF-H152-L600-SS30	152.3	6.18	159.6	8.88	30.0	610.1	598.0	164.3	150.1	12.1	0.027	296.7	4.0	8.3
IOF-H152-L750-SS30	151.8	6.13	159.8	8.68	30.0	762.6	750.5	160.5	149.5	12.1	0.030	275.0	4.1	9.5
IOF-H102-L300-SS5	101.4	4.89	67.9	5.10	5.0	311.1	299.0	110.0	89.9	12.1	0.046	126.7	7.0	10.3
IOF-H102-L300-SS7.5	101.9	4.98	67.9	5.20	7.5	311.1	299.0	110.0	89.9	12.1	0.003	132.3	5.6	8.5
IOF-H102-L300-SS10	100.8	4.92	67.8	5.19	10.0	311.1	299.0	110.0	89.9	12.1	0.031	121.8	4.0	6.5
IOF-H102-L300-SS12.5	101.3	4.94	67.9	5.17	12.5	310.1	298.0	110.0	90.0	12.1	0.043	143.2	5.2	8.7
IOF-H102-L300-SS15	101.9	4.99	67.8	5.12	15.0	310.1	298.0	110.0	89.8	12.1	0.064	130.8	3.0	5.5
IOF-H102-L300-SS20	100.9	4.91	67.8	5.10	20.0	310.6	298.5	109.9	89.8	12.1	0.002	142.5	3.2	6.2

Table 3
Summary of measured dimensions, geometric imperfections and test results of the ITF specimens.

Specimen	h (mm)	t_w (mm)	b_f (mm)	t_f (mm)	$s_s = s_h$ (mm)	L (mm)	a (mm)	h_{ep} (mm)	$b_{f,ep}$ (mm)	t_{ep} (mm)	ω_0 (mm)	F_u (kN)	δ_u (mm)
ITF-H102-L500-SS20	101.3	4.94	67.8	4.94	20.0	524.0	500.0	112.0	89.8	12.0	0.016	154.5	5.7
ITF-H102-L500-SS40	101.6	4.98	67.8	4.97	40.0	522.4	498.3	111.9	89.9	12.0	0.001	178.4	3.5
ITF-H102-L500-SS60	101.4	4.94	67.7	4.92	60.0	524.4	500.3	112.0	89.8	12.0	0.011	194.8	2.4
ITF-H102-L500-SS80	101.5	4.95	67.7	4.93	80.0	524.0	500.0	111.9	89.8	12.0	0.077	209.6	1.8
ITF-H102-L500-SS100	101.6	5.01	67.8	4.95	100.0	524.0	500.0	111.9	89.8	12.0	0.046	239.6	1.5
ITF-H160-L475-SS20	160.1	9.71	82.5	11.70	20.0	500.5	476.5	168.8	89.8	12.0	0.015	626.6	21.2
ITF-H160-L475-SS40	160.0	9.72	82.5	11.75	40.0	500.1	476.0	169.1	89.8	12.0	0.038	678.8	18.9
ITF-H160-L475-SS60	160.1	9.76	82.5	11.74	60.0	499.9	475.8	168.9	89.8	12.0	0.006	690.6	11.8

Instron 8800 750 kN hydraulic testing machine. Vertical displacement was measured by the testing machine, while the out-of-plane displacement was measured by the displacement transducer DT1. Fig. 16 shows the failure modes of all the internal two-flange test specimens. Mid-height out-of-plane web buckling failure together with significant local flange bending were observed in all cases. The load-web shortening responses of the ITF test specimens are presented in Figs. 17 and 18 while the load-out-of-plane displacement responses are plotted in Figs. 19 and 20. The key ITF test results are reported in Table 3, where δ_u is the vertical web shortening at the ultimate load taken as the displacement measured using the testing machine.

Fig. 5. Failure modes of internal one-flange (IOF) loading test specimens.

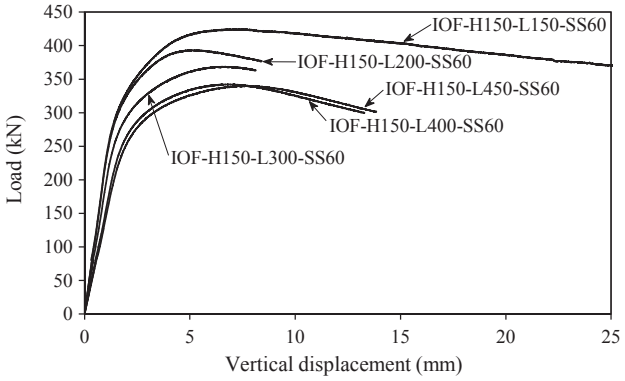

Fig. 6. Load-vertical displacement response of the tested IOF H150 specimens.

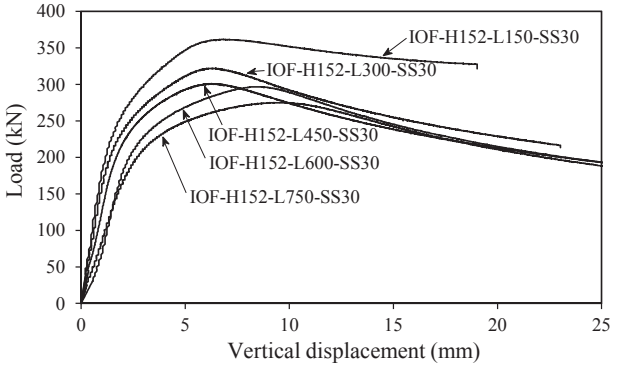

Fig. 7. Load-vertical displacement response of the tested IOF H152 specimens.

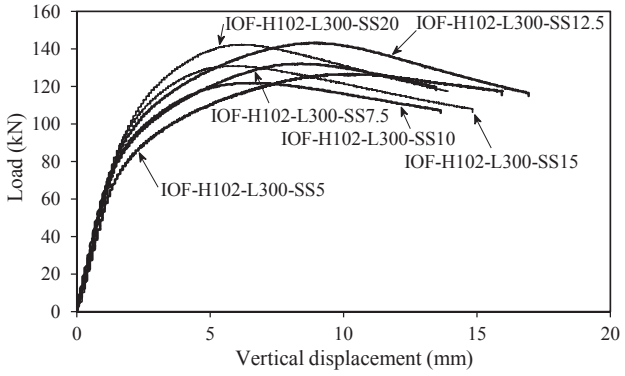

Fig. 8. Load-vertical displacement response of the tested IOF H102 specimens.

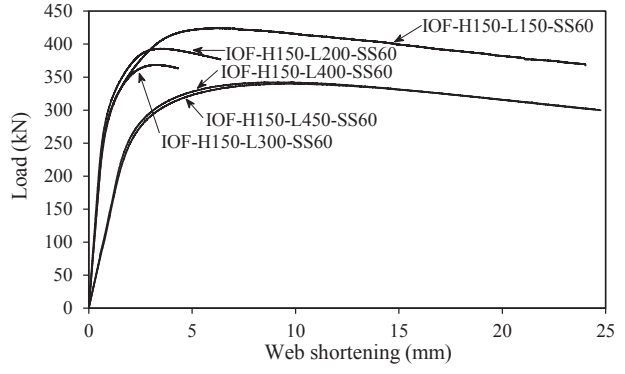

Fig. 9. Load-web shortening response of the tested IOF H150 specimens.

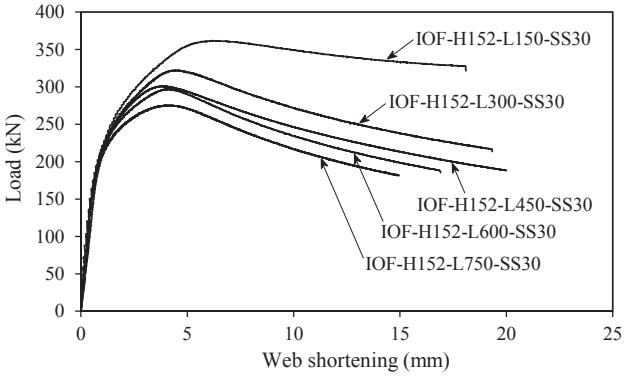

Fig. 10. Load-web shortening response of the tested IOF H152 specimens.

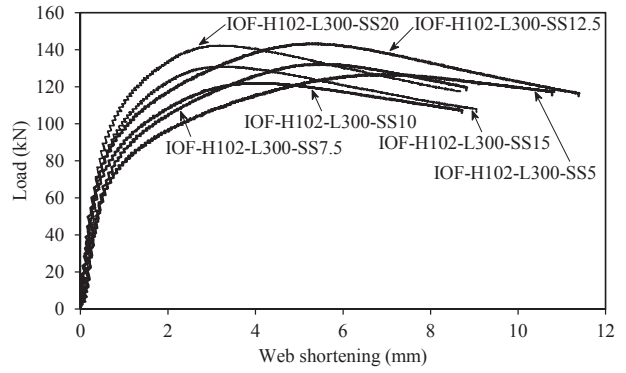

Fig. 11. Load-web shortening response of the tested IOF H102 specimens.

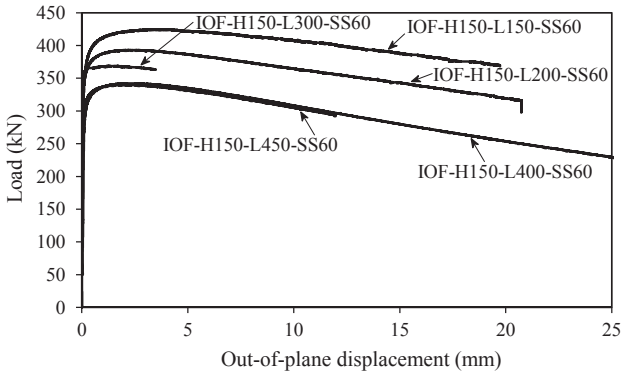

Fig. 12. Load-out-of-plane displacement response of the tested IOF H150 specimens.

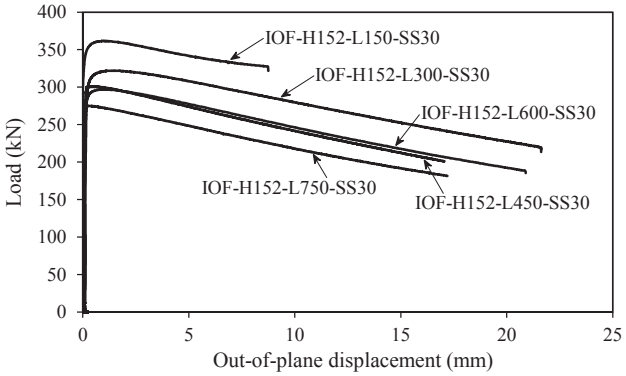

Fig. 13. Load-out-of-plane displacement response of the tested IOF H152 specimens.

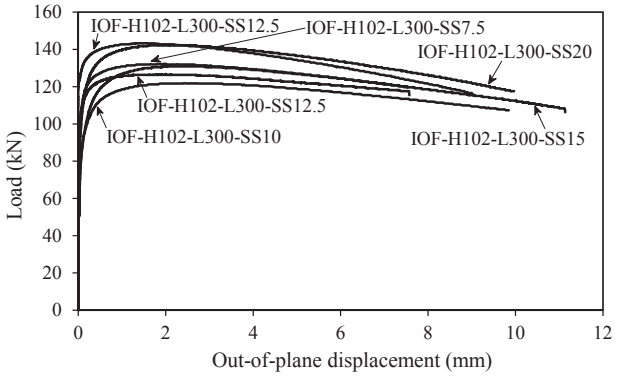

Fig. 14. Load-out-of-plane displacement response of the tested IOF H102 specimens.

Digital Image Correlation (DIC) was also employed, as described previously for the IOF specimens, to obtain the out-of-plane deformation fields of the webs of the tested ITF specimens. Fig. 21 shows the load-out-of-plane displacement response, together with the out-of-plane deformation fields obtained during the testing of specimen ITF-H102-L500-SS20. The out-of-plane deformation fields indicate that the maximum out-of-plane displacement occurred at mid-span under the point of load application but unlike for IOF test specimens, the maximum out-of-plane displacement occurred approximately at the mid-height of the web.

3. Numerical modelling

Numerical models were developed using the finite element analysis software Abaqus [47]. Initially, the full load-deformation histories and failure modes obtained from the experiments were used to validate the numerical models and assess their sensitivity to various input parameters. Further parametric studies were then carried out to extend the experimental database.

3.1. Modelling assumptions

The four-noded shell element with reduced integration, referred to as S4R in the Abaqus element library [47], was used to mesh the beams and endplates, while the eight-noded linear solid element with reduced integration, referred to as C3D8R in the Abaqus element library [47], was used to model the bearing plates. A uniform element size approximately equal to half the web thickness of the considered I-sections was adopted for all features of the models (i.e. bearing plates, I-section and end plates), following a preliminary mesh sensitivity study. The measured engineering material stress-strain curves obtained from the tensile coupon tests described in Section 2.1 [42] were converted into the form of true stress and log plastic strain according to Eqs. (1) and (2), where σ_{true} is the true stress, ε_{ln}^{pl} is the true plastic strain, E is the Young's modulus, σ_{nom} and ε_{nom} are the engineering stress and the engineering strain, respectively, before input into the finite element models. The measured engineering stress-strain curve and the true stress-strain curve for the material extracted from each of the tested cross-sections are shown in Fig. 22.

$$\sigma_{true} = \sigma_{nom}(1 + \varepsilon_{nom}) \tag{1}$$

$$\varepsilon_{ln}^{pl} = \ln(1 + \varepsilon_{nom}) - \frac{\sigma_{true}}{E} \tag{2}$$

Elastic material behaviour was adopted for the end plates, with a Young's modulus E of 210,000 MPa and a Poisson's ratio ν of 0.3. The bearing plate was simulated as a rigid block by constraining all its degrees of freedom to a reference point where the load was applied. The boundary conditions of the models were defined to reflect the two test setups: for the IOF loading models, as shown in Fig. 23 (a), the vertical (U2) and out-of-plane (U1) displacements, as well as the rotations about the vertical (UR2) and longitudinal (UR3) axes at the bottom of each end plate were restrained; for the ITF loading models, as shown in Fig. 23 (b), the out-of-plane displacement (U1) was restrained at four end plate nodes, while in all the models, the longitudinal displacement (U3) was restrained at the mid-length of the top flange, providing symmetry in the boundary conditions, as in the tests.

The interaction between the bearing plate and the top flange of the I-sections beneath the applied loading was taken into account by defining surface-to-surface contact between the bearing plate (master surface) and the I-section flange (slave surface). A finite sliding procedure [47] was adopted which allows arbitrary motion of both surfaces. A friction coefficient of 0.4 was used for the tangential contact properties while for the normal contact properties, a "hard" contact relationship was adopted, which assumes that the contact pressure-

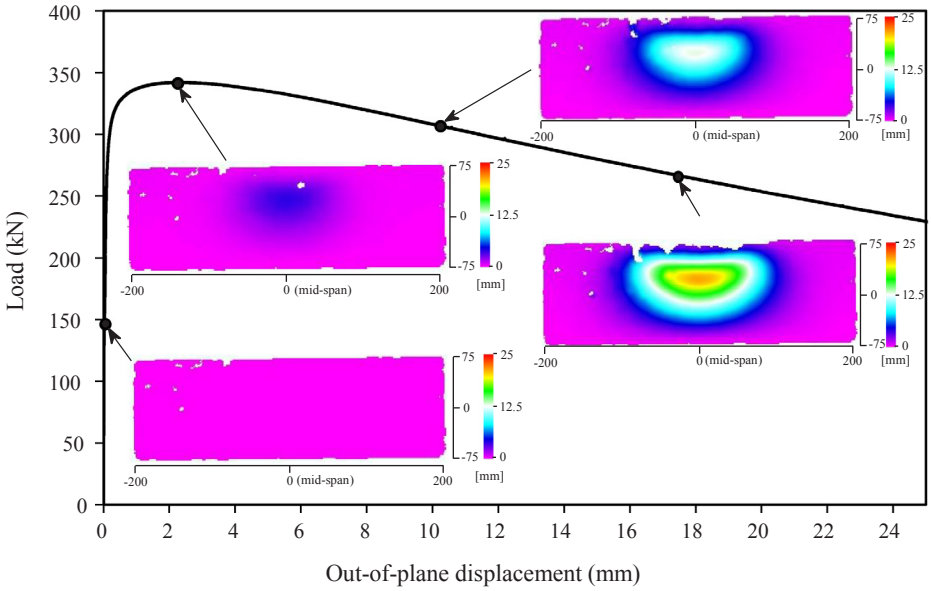

Fig. 15. Load-out-of-plane displacement response of test specimen IOF-H150-L400-SS60 and corresponding out-of-plane web deformation fields obtained using Digital Image Correlation.

Fig. 16. Failure modes of internal two-flange (ITF) loading test specimens.

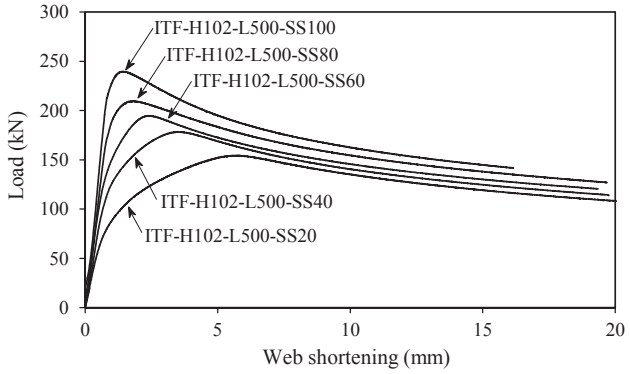

Fig. 17. Load-web shortening response of the tested ITF H102 specimens.

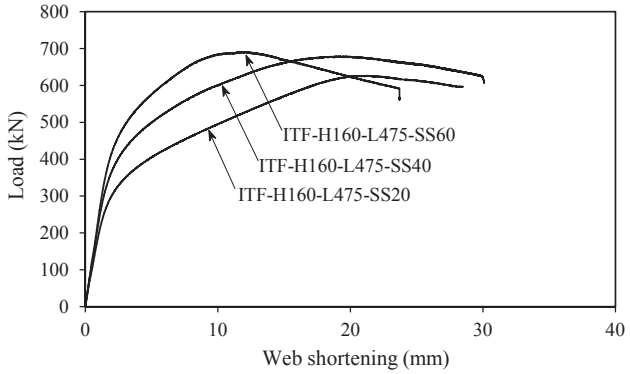

Fig. 18. Load-web shortening response of the tested ITF H160 specimens.

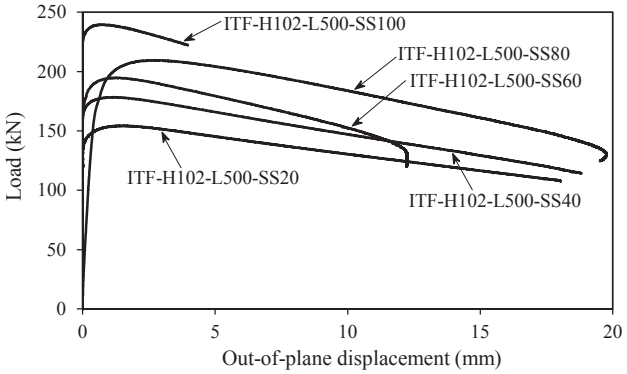

Fig. 19. Load-out-of-plane displacement response of the tested ITF H102 specimens.

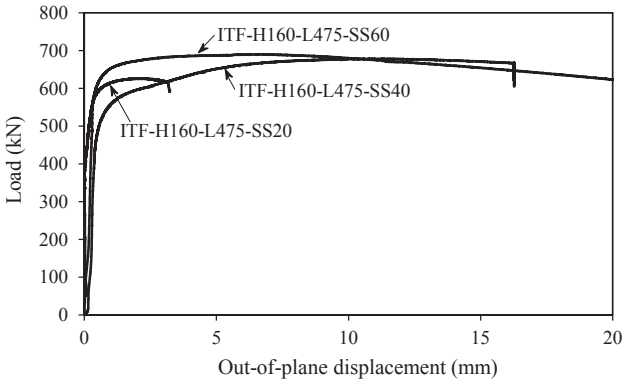

Fig. 20. Load-out-of-plane displacement response of the tested ITF H160 specimens.

overclosure relationship is dictated by the stiffness of each of the parts in contact with each other [47].

During the fabrication process, laser-welded I-sections are subjected to thermal gradients which lead to the development of residual stresses during the cooling phase. A predictive model for residual stresses in laser-welded I-sections was proposed in [42,48]. However, a preliminary study into their influence on the structural response under concentrated loading revealed very low sensitivity; a similar finding was reported for the cross-section resistance of stainless steel welded I-sections in bending [49], and residual stresses were thus not explicitly incorporated into the numerical models developed herein. Initial local geometric imperfections were accounted for by defining imperfection

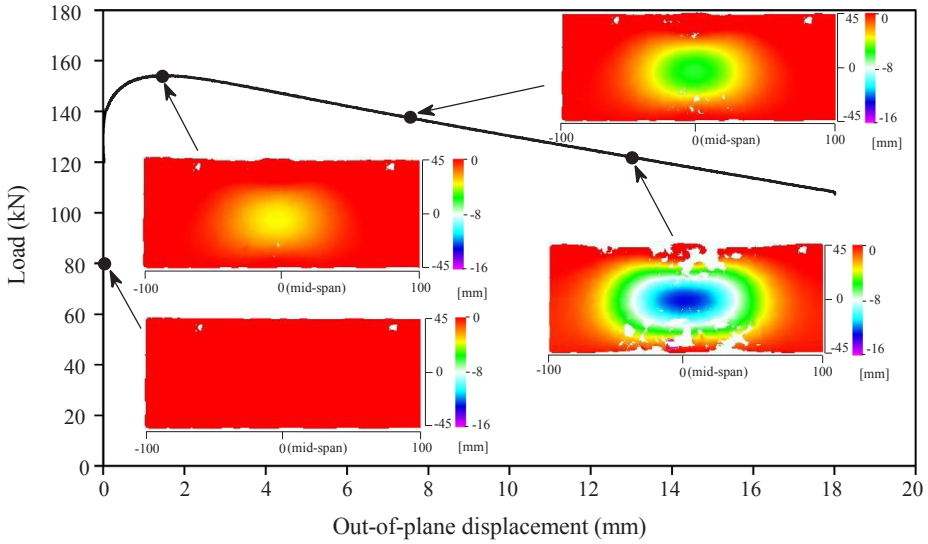

Fig. 21. Load-out-of-plane displacement response of test specimen ITF-H102-L500-SS20 and corresponding out-of-plane web deformation fields obtained using Digital Image Correlation.

patterns in the form of the first buckling mode shapes obtained from prior linear eigenvalue buckling analyses. A sensitivity study was performed to investigate the influence of four different imperfection amplitudes ω_0 on the structural response of the modelled I-sections: (i) the value measured for each specimen in the experiments ω_0 using the procedure described in Section 2.2 and, (ii) 1/100, (iii) 1/300, and (iv) 1/500 of the cross-section web thickness. Following incorporation of the initial geometric imperfections into the numerical models, geometrically and materially non-linear analyses (GMNIA) were carried out using the modified Riks solver [47] to obtain the full load-deformation response of the specimens, including the post-peak behaviour.

3.2. Validation of finite element models

The accuracy of the finite element (FE) models was assessed by comparing their load-web-shortening responses, ultimate load predictions, web shortening values at the ultimate loads and failure modes against those observed of the experiments. The ultimate load and corresponding web shortening values, considering the four imperfection amplitudes in the numerical models, are reported in Table 4 for the IOF

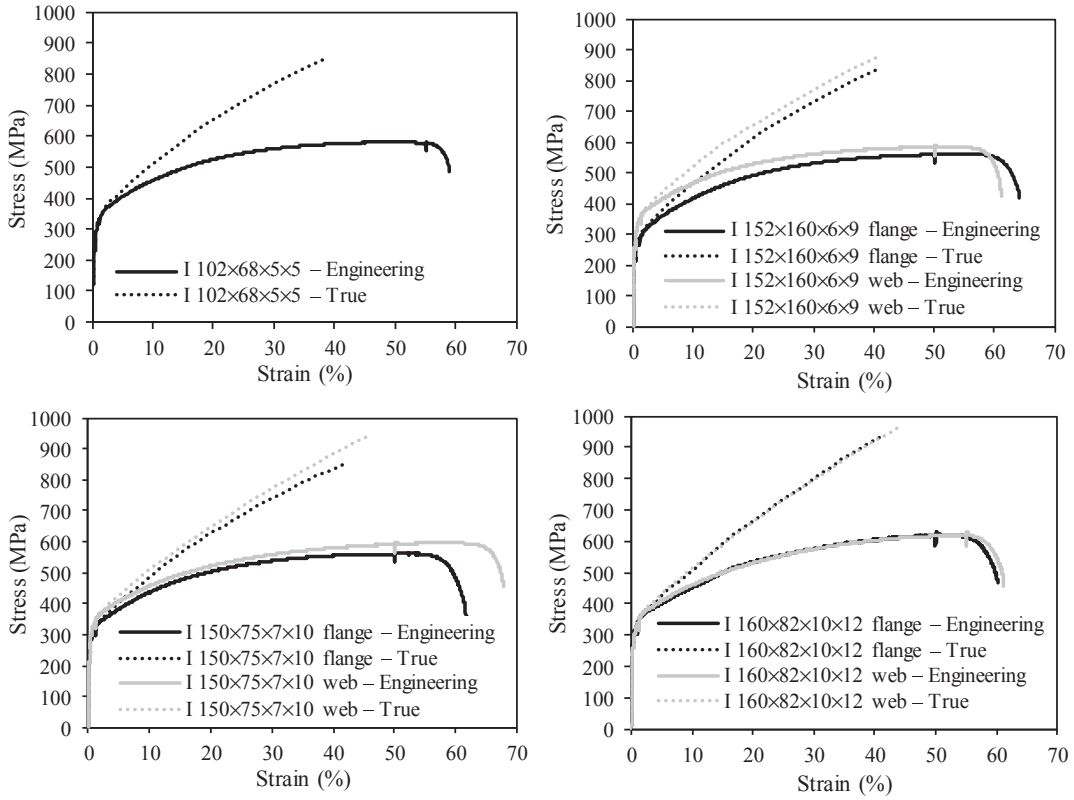

Fig. 22. Engineering and true stress-strain curves for material from tested cross-sections.

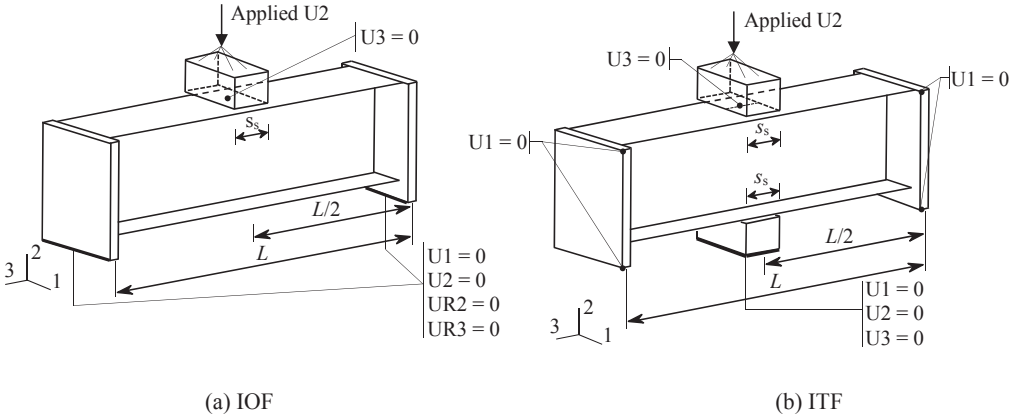

Fig. 23. Boundary conditions adopted in the finite element models.

Table 4
Comparison of the IOF test results with FE results for different imperfection amplitudes.

Specimen	Measured amplitude		$t_w/100$		$t_w/300$		$t_w/500$	
	$F_{u,FE}/F_{u,Test}$	$\delta_{u,FE}/\delta_{u,Test}$	$F_{u,FE}/F_{u,Test}$	$\delta_{u,FE}/\delta_{u,Test}$	$F_{u,FE}/F_{u,Test}$	$\delta_{u,FE}/\delta_{u,Test}$	$F_{u,FE}/F_{u,Test}$	$\delta_{u,FE}/\delta_{u,Test}$
IOF-H150-L150-SS60	0.99	0.59	0.97	0.47	0.99	0.48	1.00	0.51
IOF-H150-L200-SS60	1.01	1.05	0.99	0.66	1.01	0.73	1.06	0.81
IOF-H150-L300-SS60	1.01	1.36	1.00	0.61	1.01	0.62	1.02	0.62
IOF-H150-L400-SS60	1.04	0.59	1.02	0.22	1.02	0.19	1.03	0.21
IOF-H150-L450-SS60	1.03	0.64	1.01	0.17	1.01	0.19	1.01	0.17
IOF-H152-L150-SS30	1.05	0.79	0.96	0.58	1.00	0.70	1.02	0.64
IOF-H152-L300-SS30	0.96	0.93	0.93	0.57	0.95	0.66	0.96	0.65
IOF-H152-L450-SS30	1.01	1.47	0.96	0.69	0.99	0.78	1.01	0.86
IOF-H152-L600-SS30	0.96	1.53	0.93	0.62	0.95	0.69	0.96	0.68
IOF-H152-L750-SS30	0.95	1.69	0.92	0.53	0.94	0.58	0.95	0.65
IOF-H102-L300-SS5	0.96	0.97	0.95	0.65	0.99	0.68	0.99	0.72
IOF-H102-L300-SS7.5	1.03	1.49	0.96	0.75	0.99	0.77	1.01	0.80
IOF-H102-L300-SS10	1.05	1.52	1.05	0.89	1.07	0.94	1.09	1.03
IOF-H102-L300-SS12.5	0.92	1.08	0.92	0.63	0.94	0.70	0.95	0.70
IOF-H102-L300-SS15	1.02	1.69	1.04	1.01	1.06	1.11	1.07	1.14
IOF-H102-L300-SS20	1.02	1.98	0.96	0.82	0.99	0.91	1.00	0.94
Mean	1.00	1.21	0.97	0.62	0.99	0.67	1.01	0.70
COV	0.04	0.36	0.04	0.35	0.04	0.36	0.04	0.37

loading cases, and in Table 5 for the ITF loading cases. As can be seen from the table, the ultimate load and corresponding web shortening values obtained from the numerical models are very close to those of the tested specimens. The best agreement between the test and finite element results was obtained for an imperfection amplitude of $t_w/500$ for both loading cases; hence, an amplitude of $t_w/500$ is adopted in the numerical models for the parametric studies described in the following section. Excellent agreement is also observed between the numerical and experimental failure modes for both loading conditions, as shown in Fig. 24 for a typical IOF loading specimen and Fig. 25 for a typical ITF loading specimen. Typical numerical and experimental load versus web shortening responses and load versus out-of-plane displacement responses for the IOF and ITF loading cases are shown in Figs. 26–29. These comparisons show generally good agreement over the full load-deformation history, including initial stiffness, ultimate load and post-ultimate response.

Table 5
Comparison of the ITF test results with FE results for different imperfection amplitudes.

Specimen	Measured amplitude		$t_w/100$		$t_w/300$		$t_w/500$	
	$F_{u,FE}/F_{u,Test}$	$\delta_{u,FE}/\delta_{u,Test}$	$F_{u,FE}/F_{u,Test}$	$\delta_{u,FE}/\delta_{u,Test}$	$F_{u,FE}/F_{u,Test}$	$\delta_{u,FE}/\delta_{u,Test}$	$F_{u,FE}/F_{u,Test}$	$\delta_{u,FE}/\delta_{u,Test}$
ITF-H102-L500-SS20	0.97	0.82	0.92	0.72	0.96	0.81	0.98	0.88
ITF-H102-L500-SS40	0.98	0.85	0.90	0.62	0.92	0.74	0.93	0.72
ITF-H102-L500-SS60	0.94	0.66	0.92	0.59	0.93	0.64	0.94	0.67
ITF-H102-L500-SS80	0.94	0.58	0.95	0.59	1.02	0.70	1.03	0.69
ITF-H102-L500-SS100	0.95	0.63	0.95	0.62	0.98	0.73	0.99	0.74
ITF-H160-L475-SS20	0.96	0.75	0.89	0.64	0.93	0.70	0.95	0.74
ITF-H160-L475-SS40	0.90	0.51	0.87	0.46	0.91	0.53	0.92	0.54
ITF-H160-L475-SS60	0.98	0.68	0.90	0.51	0.94	0.56	0.95	0.60
Mean	0.95	0.68	0.91	0.59	0.95	0.67	0.96	0.70
COV	0.03	0.17	0.03	0.13	0.04	0.14	0.04	0.15

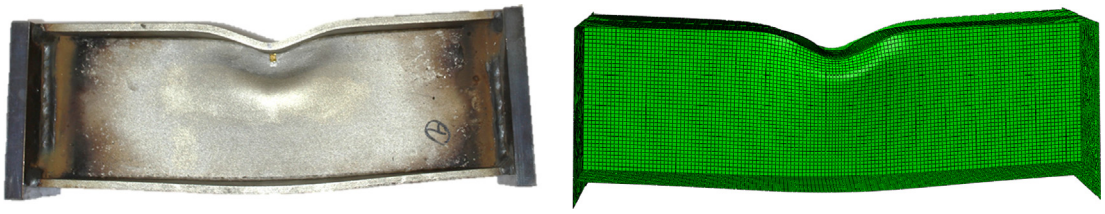

Fig. 24. Experimental and numerical failure modes of specimen IOF-H102-L300-SS12.5.

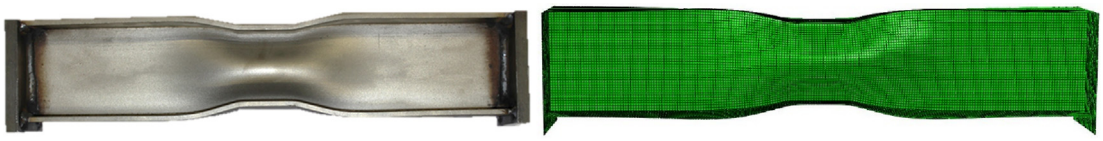

Fig. 25. Experimental and numerical failure modes of specimen ITF-H102-L500-SS60.

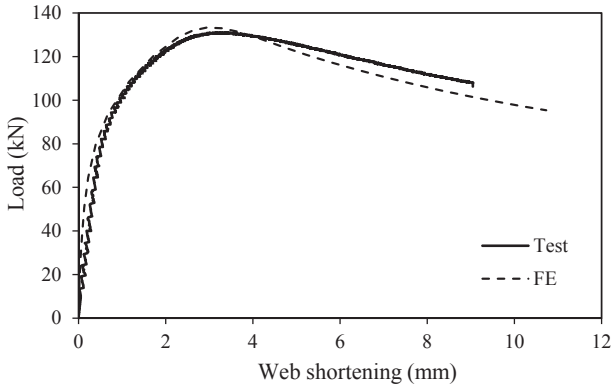

Fig. 26. Experimental and numerical load-web shortening responses of the IOF-H102-L300-SS15 specimen.

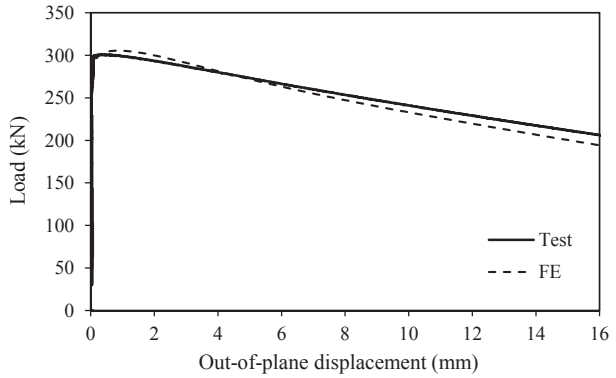

Fig. 27. Experimental and numerical load-out-of-plane displacement response of the IOF-H152-L450-SS30 specimen.

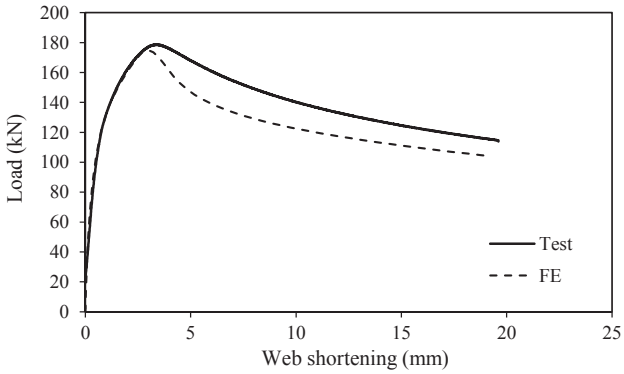

Fig. 28. Experimental and numerical load-web shortening response of the ITF-H102-L500-SS40 specimen.

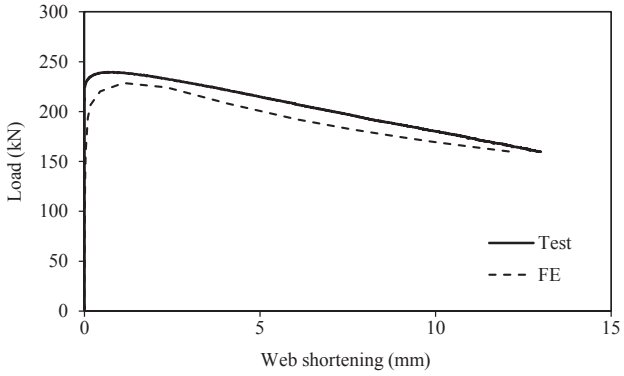

Fig. 29. Experimental and numerical load-out-of-plane displacement response of the ITF-H102-L500-SS100 specimen.

3.3. Parametric studies

Following validation of the finite element models against the test results, parametric studies were performed to evaluate the influence of a range of key parameters on the web bearing resistances of welded stainless steel I-sections under internal one-flange (IOF) loading and internal two-flange (ITF) loading. In these studies, the measured material properties of the I 102 × 68 × 5 × 5 specimen (see Table 1) were adopted, with the initial geometric imperfection in the form of the first buckling mode scaled with a maximum amplitude of 1/500 of the cross-section web thickness t_w (i.e. t_w/500). The web height (h_w), flange thickness (t_f) and flange width (b_f) were kept constant and taken as equal to h_w = 200 mm, t_f = 5.2 mm and b_f = 67.8 mm for both loading conditions. A member length of 350 mm was adopted for the IOF models, while a member length of 500 mm was used for the ITF models in the parametric studies. The web thickness (t_w) and the bearing length (s_s) values were varied to cover a range of web slendernesses (h_w/t_w) from 10 to 120 and a range of ratios of bearing length to web height (s_s/h_w) from 0.05 to 1.20. The influence of these parameters is assessed in the following two sub-sections.

3.3.1. Influence of bearing length

The influence of bearing length s_s on the ultimate web bearing resistances of the modelled I-section members under IOF and ITF loading is shown in Figs. 30 and 31, respectively. The same data are plotted on two different scales on the vertical axis (which shows the ultimate load F_u) in (a) and (b) to distinguish better between the data points with

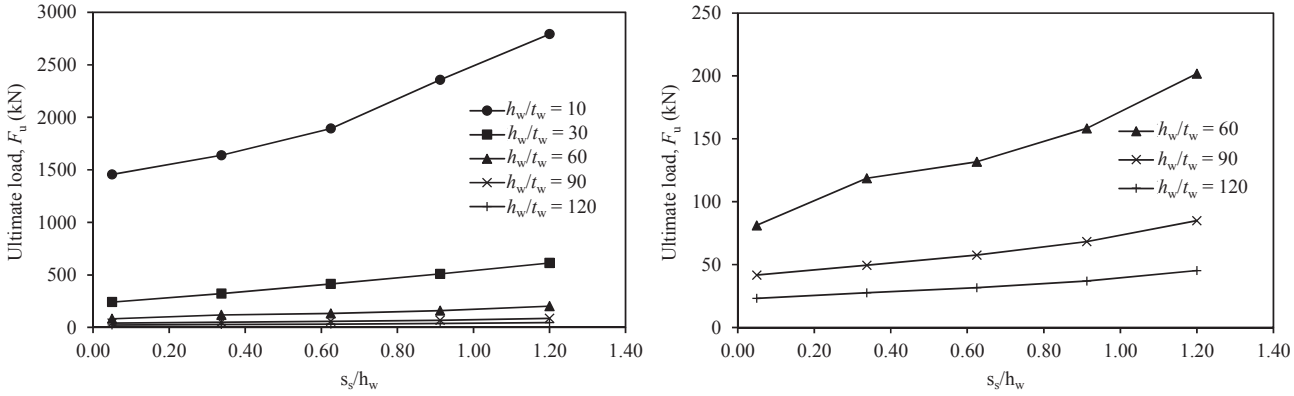

(a) Vertical axis scale up to 3000 kN (b) Vertical axis scale up to 250 kN

Fig. 30. Influence of bearing length (s_s), normalized by web height, on ultimate load of IOF models for different web slenderness (h_w/t_w).

lower failure loads. On the horizontal axis, the bearing length is normalised by the web height (i.e. s_s/h_w). For both loading types, the ultimate load may be seen to increase almost linearly with increasing bearing length, due to the load being spread of a larger region of the web.

3.3.2. Influence of web slenderness

The influence of web slenderness on the ultimate resistance of the modelled I-section members for different bearing lengths is shown in Figs. 32 and 33 for IOF and ITF loading, respectively, in which the web slenderness h_w/t_w is plotted on the horizontal axis while the ultimate load F_u is again plotted at two different scales in (a) and (b) on the vertical axis. For both loading cases, the ultimate load may be seen to reduce sharply with increasing web slenderness, particularly for h_w/t_w values less than 60.

4. Assessment of existing design rules

In this section, the methods provided in the European code EN 1993-1-4 [50] and in the American AISC Design Guide 27 [40] for the design of stainless steel members under concentrated transverse loading are described and assessed. The accuracy of the design provisions is evaluated by comparing the experimental and numerical failure loads (F_u) against the ultimate loads predicted by the specification ($F_{u,pred}$), utilising the recommended design interaction curves for resistance to combined concentrated loading and bending moment assuming proportional loading (see Fig. 34) for the internal one-flange (IOF) loading case. For the internal two-flange (ITF) loading case, the predicted ultimate loads ($F_{u,pred}$) are compared directly with the experimental and numerical ultimate loads. A value for $F_u/F_{u,pred}$ greater than unity indicates a safe-sided design prediction. Note that the measured (or modelled) material and geometric properties were used in all the comparisons and that all partial safety factors were set equal to unity.

4.1. European design provisions: EN 1993-1-4 (EC3)

EN 1993-1-4 [50] adopts the carbon steel design rules set out in EN 1993-1-5 [39] for stainless steel members under concentrated loading. The design resistance to local failure under concentrated transverse loading F_{Rd} is determined using Eq. (3), where f_{yw} is the web 0.2% proof stress, t_w is the web thickness and L_{eff} is the effective length, which is given by the product of effective loaded length l_y from Eq. (4) and the reduction factor χ_F. The method adopted for the determination of the effective loaded length l_y is based on the four-hinge plastic mechanism model originally proposed by Roberts and Rockey [51]. The reduction factor χ_F, determined from Eq. (5) is a function of the slenderness parameter $\overline{\lambda}_F$, which is equal to the square root of the ratio of the plastic load (Eq. (6)) to the elastic buckling load F_{cr} of the member under concentrated force. The buckling load is determined from Eq. (7) where k_F is the buckling coefficient, which has different values for different transverse loading types (i.e. IOF, ITF etc), and a is the distance between stiffeners taken as the span excluding the end plate thickness (i.e. $a = L - t_{ep}$).

$$F_{Rd} = f_{yw} L_{eff} t_w \quad \text{where} \quad L_{eff} = \chi_F l_y \tag{3}$$

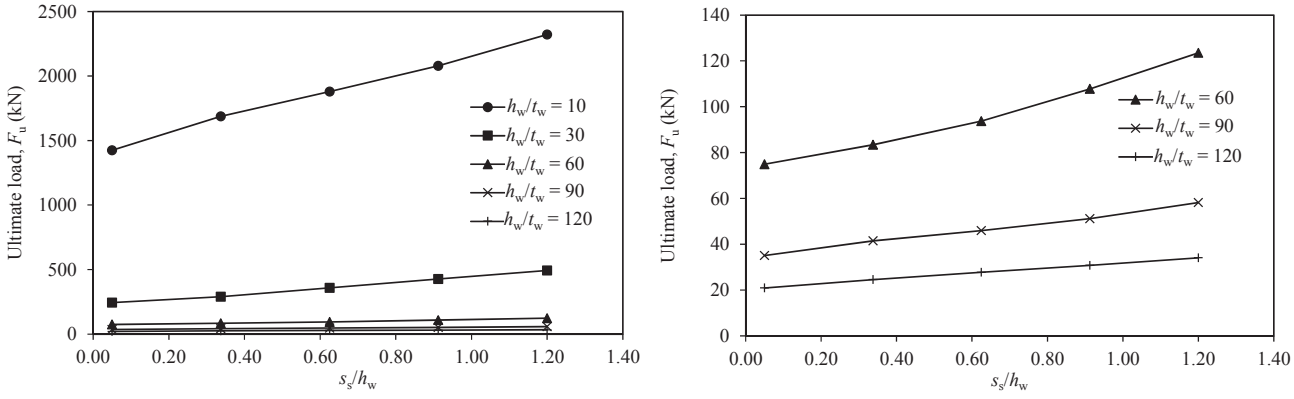

(a) Vertical axis scale up to 2500 kN (b) Vertical axis scale up to 140 kN

Fig. 31. Influence of bearing length (s_s), normalized by web height, on ultimate load of ITF models for different web slenderness (h_w/t_w).

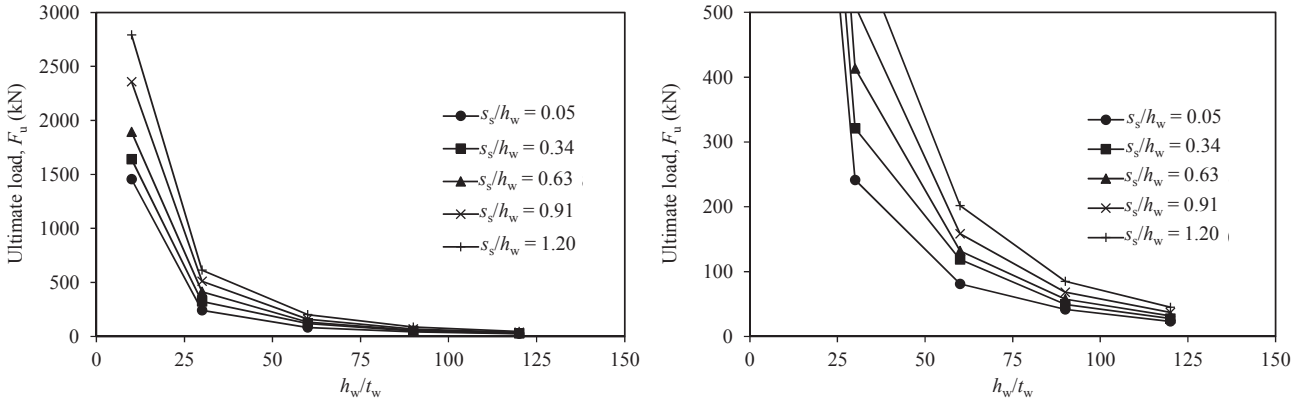

Fig. 32. Influence of web slenderness (h_w/t_w) on ultimate load of IOF models for different bearing length to web-height ratios.

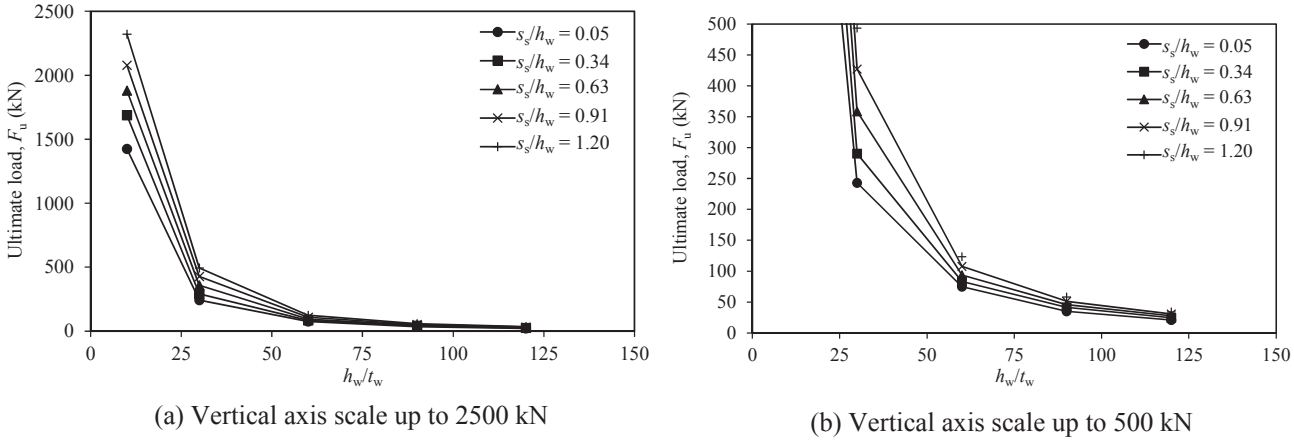

Fig. 33. Influence of web slenderness (h_w/t_w) on ultimate load of ITF models for different bearing length to web-height ratios.

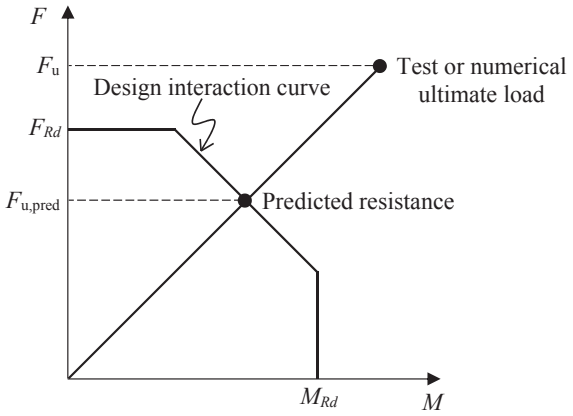

Fig. 34. Definition of F_u and $F_{u,pred}$ for IOF loading case.

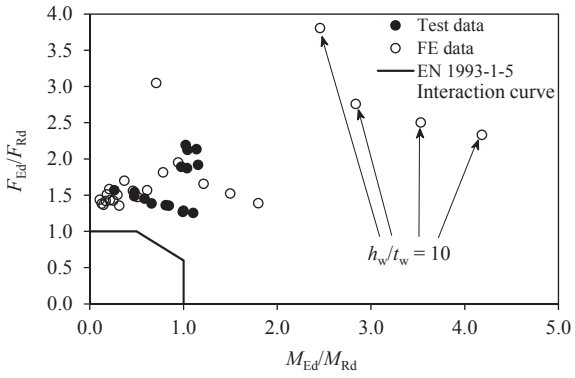

Fig. 35. Comparison of IOF test and FE results with EN 1993-1-5 F-M interaction diagram.

$$l_y = s_s + 2t_f(1 + \sqrt{m_1 + m_2})$$

$$\text{where} \quad m_1 = \frac{f_{yf}\, b_f}{f_{yw}\, t_w} \quad \text{and} \quad m_2 = \begin{cases} 0.02\left(\frac{h_w}{t_f}\right)^2 \text{for } \bar{\lambda}_F > 0.5 \\ 0 \text{for } \bar{\lambda}_F \leqslant 0.5 \end{cases} \tag{4}$$

$$\chi_F = \frac{0.5}{\bar{\lambda}_F} \leqslant 1.0 \quad \text{where} \quad \bar{\lambda}_F = \sqrt{\frac{F_y}{F_{cr}}} \tag{5}$$

$$F_y = l_y\, t_w f_{yw} \tag{6}$$

$$F_{cr} = 0.9\, k_F\, E\, \frac{t_w^3}{h_w} \quad \text{where} \quad k_F = \begin{cases} 6 + 2\left(\frac{h_w}{a}\right)^2 \text{for IOF loading} \\ 3.5 + 2\left(\frac{h_w}{a}\right)^2 \text{for ITF loading} \end{cases} \tag{7}$$

In the case of a member subjected to concentrated transverse loading plus bending moment (i.e. internal one-flange (IOF) loading), the interaction between the forces should be considered through Eq. (8), where F_{Ed} is the applied concentrated transverse force, F_{Rd} is the design resistance to concentrated transverse loading given by Eq. (3), M_{Ed} is the applied bending moment and $M_{pl,Rd}$ is the plastic bending moment resistance of the cross-section regardless of its classification

Table 6
Design resistance of members under concentrated transverse loading according to AISC 360–16 [53].

Limit state	Resistance formulae
Web yielding AISC 360-16 [53], J10.2	If load is applied at a distance greater than h from the member end: $F_{Rd} = f_{yw}\, t_w\,(5k + s_s)$ If load is applied at a distance equal or less than h from the member end: $F_{Rd} = f_{yw}\, t_w\,(2.5k + s_s)$ where k is the distance from the outer face of the flange to the web fillet toe.
Web crippling AISC 360-16 [53], J10.3	If load is applied at a distance greater or equal to $h/2$ from the member end: $F_{Rd} = 0.80 t_w^2 \left[1 + 3\left(\frac{s_s}{h}\right)\left(\frac{t_w}{t_f}\right)^{1.5}\right]\sqrt{\frac{E f_{yw}\, t_f}{t_w}}$ If load is applied at a distance less than $h/2$ from the member end: For $s_s/h \leqslant 0.2$: $F_{Rd} = 0.40 t_w^2 \left[1 + 3\left(\frac{s_s}{h}\right)\left(\frac{t_w}{t_f}\right)^{1.5}\right]\sqrt{\frac{E f_{yw}\, t_f}{t_w}}$ For $s_s/h > 0.2$: $F_{Rd} = 0.40 t_w^2 \left[1 + \left(\frac{4 s_s}{h} - 0.2\right)\left(\frac{t_w}{t_f}\right)^{1.5}\right]\sqrt{\frac{E f_{yw}\, t_f}{t_w}}$
Web buckling AISC 360–16 [53], J.10.5 (for ITF only)	If load is applied at a distance equal or greater than $h/2$ from the member end: $F_{Rd} = \left(\frac{24 t_w^3 \sqrt{E f_{yw}}}{h_w}\right)$ If load is applied at a distance less than $h/2$ from the member end: $F_{Rd} = \frac{1}{2}\left(\frac{24 t_w^3 \sqrt{E f_{yw}}}{h_w}\right)$

Table 7
Comparisons of the IOF test and FE results with the ultimate web bearing strengths predicted by EN 1993-1-5 (EC3) and AISC 360-16.

(a) All cases		
No. of tests: 16	$F_u/F_{u,EC3}$	$F_u/F_{u,AISC}$
No. of FE simulations: 24		
Mean	1.91	2.42
COV	0.40	0.44
(b) $h_w/t_w = 10$		
No. of tests: 0	$F_u/F_{u,EC3}$	$F_u/F_{u,AISC}$
No. of FE simulations: 4		
Mean	3.53	3.04
COV	0.26	0.27
(c) $18 < h_w/t_w \leq 22$		
No. of tests: 16	$F_u/F_{u,EC3}$	$F_u/F_{u,AISC}$
No. of FE simulations: 0		
Mean	1.69	2.60
COV	0.18	0.24
(d) $h_w/t_w = 30$		
No. of tests: 0	$F_u/F_{u,EC3}$	$F_u/F_{u,AISC}$
No. of FE simulations: 5		
Mean	2.17	2.87
COV	0.23	0.70
(e) $h_w/t_w = 60$		
No. of tests: 0	$F_u/F_{u,EC3}$	$F_u/F_{u,AISC}$
No. of FE simulations: 5		
Mean	1.56	2.18
COV	0.11	0.56
(f) $h_w/t_w = 90$		
No. of tests: 0	$F_u/F_{u,EC3}$	$F_u/F_{u,AISC}$
No. of FE simulations: 5		
Mean	1.51	1.87
COV	0.07	0.49
(g) $h_w/t_w = 120$		
No. of tests: 0	$F_u/F_{u,EC3}$	$F_u/F_{u,AISC}$
No. of FE simulations: 5		
Mean	1.44	1.63
COV	0.06	0.41

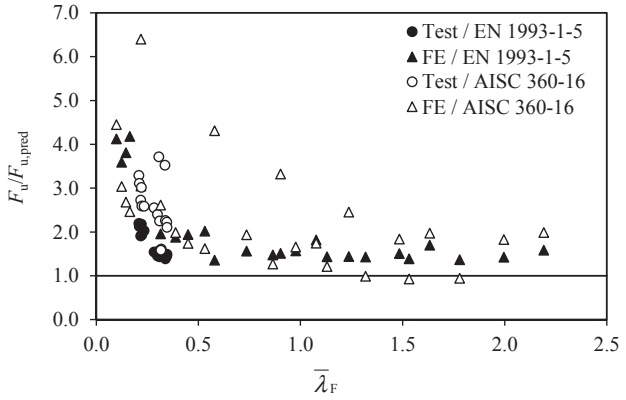

Fig. 36. Comparison of IOF loading test and FE results against the European and North American design resistance predictions.

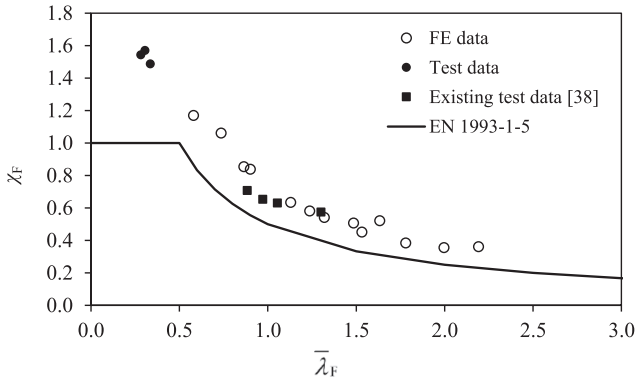

Fig. 37. Comparison of ultimate strengths determined from IOF loading tests and FE simulations against EN 1993-1-5 design curve.

(compactness). Note that the maximum attainable bending moment resistance M_{Rd} is still limited to the plastic, elastic or effective moment capacity for Class 1–2, Class 3 and Class 4 cross-sections, respectively.

$$\frac{F_{Ed}}{F_{Rd}} + 0.8\frac{M_{Ed}}{M_{pl,Rd}} \leqslant 1.4 \tag{8}$$

The experimental and numerical ultimate capacities for the case of internal one-flange (IOF) loading are plotted on the EC3 interaction diagram in Fig. 35. The comparisons reveal the safe-sided, but generally overly-conservative nature of the EN 1993-1-5 (EN 1993-1-4) resistance predictions for stainless steel I-sections, particularly with decreasing web slenderness$\overline{\lambda}_F$. A quantitative evaluation of the accuracy of the EN 1993-1-5 resistance predictions for the IOF loading case can be found in Table 7, which shows a mean $F_u/F_{u,EC3}$ value of 1.91 with a coefficient of variation (COV) of 0.44 for all the studied cases. The table also shows increasing $F_u/F_{u,EC3}$ ratios for the stockier sections (e.g. $F_u/F_{u,EC3} = 3.53$ for $h_w/t_w = 10$ in comparison to $F_u/F_{u,EC3} = 1.44$ for $h_w/t_w = 120$). The overly-conservative results for the stockier sections, also observed in Fig. 36, are attributed to the neglect of the pronounced strain hardening exhibited by stainless steel members with stocky webs. Such behaviour has also be observed for stocky stainless steel cross-sections in other loading configurations [45,49] and addressed by means of the deformation based continuous strength method [52]. Fig. 37 shows a comparison of the EN 1993-1-5 strength curve for concentrated transverse loading, i.e. the reduction factor χ_F, given by Eq. (5) versus the non-dimensional slenderness $\overline{\lambda}_F$, and the IOF test and FE results. The IOF test data of Sélen [38] on welded stainless steel I-sections are also included in the figure. Note that only results where failure under concentrated loading (rather than bending) is dominant are shown, which is deemed to be the case according to the EN 1993-1-

Table 8
Comparisons of ITF test and FE results with the ultimate web bearing strengths predicted by EN 1993-1-4 (EC3) and AISC 360-16.

(a) All cases		
No. of tests: 8	$F_u/F_{u,EC3}$	$F_u/F_{u,AISC}$
No. of FE simulations: 24		
Mean	1.80	3.87
COV	0.32	0.58
(b) $h_w/t_w = 10$		
No. of tests: 0	$F_u/F_{u,EC3}$	$F_u/F_{u,AISC}$
No. of FE simulations: 4		
Mean	2.70	2.82
COV	0.32	0.83
(c) $18 < h_w/t_w \leq 22$		
No. of tests: 8	$F_u/F_{u,EC3}$	$F_u/F_{u,AISC}$
No. of FE simulations: 0		
Mean	1.81	2.27
COV	0.24	0.29
(d) $h_w/t_w = 30$		
No. of tests: 0	$F_u/F_{u,EC3}$	$F_u/F_{u,AISC}$
No. of FE simulations: 5		
Mean	1.81	2.35
COV	0.40	0.40
(e) $h_w/t_w = 60$		
No. of tests: 0	$F_u/F_{u,EC3}$	$F_u/F_{u,AISC}$
No. of FE simulations: 5		
Mean	1.46	3.36
COV	0.07	0.20
(f) $h_w/t_w = 90$		
No. of tests: 0	$F_u/F_{u,EC3}$	$F_u/F_{u,AISC}$
No. of FE simulations: 5		
Mean	1.55	5.45
COV	0.05	0.19
(g) $h_w/t_w = 120$		
No. of tests: 0	$F_u/F_{u,EC3}$	$F_u/F_{u,AISC}$
No. of FE simulations: 5		
Mean	1.61	7.69
COV	0.04	0.19

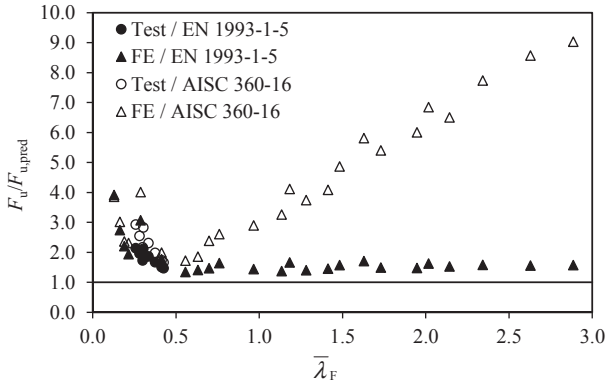

Fig. 38. Comparison of ITF loading test and FE results against the European and North American resistance predictions.

5 interaction formula when $M_u < 0.5M_{pl}$. The conservatism of the EN 1993-1-5 provisions is evident over the full analysed slenderness range, but particularly for the more stocky cross-sections.

For the members under ITF loading, Table 8 and Fig. 38 provide a comparison of the experimental and numerical failure loads F_u with the predicted failure loads according to EN 1993-1-5 $F_{u,EC3}$. The mean value of $F_u/F_{u,EC3}$ is equal to 1.80 with a coefficient of variation (COV) of 0.32, again indicating substantial conservatism in the current Eurocode design provisions. The ITF loading test and FE results are plotted against the EN 1993-1-5 strength curve in Fig. 39, revealing, together with Fig. 38, discrepancies between the reference results and the EN 1993-1-5 predicted values are most significant for stockier cross-sections (i.e. from $h_w/t_w = 10$ to $h_w/t_w = 30$). It should be noted also that an increase in $F_u/F_{u,EC3}$ values is observed for cross-sections with slender webs relative to those with webs of moderate slenderness (i.e. $F_u/F_{u,EC3} = 1.55$ for $h_w/t_w = 90$ and $F_u/F_{u,EC3} = 1.61$ for $h_w/t_w = 120$).

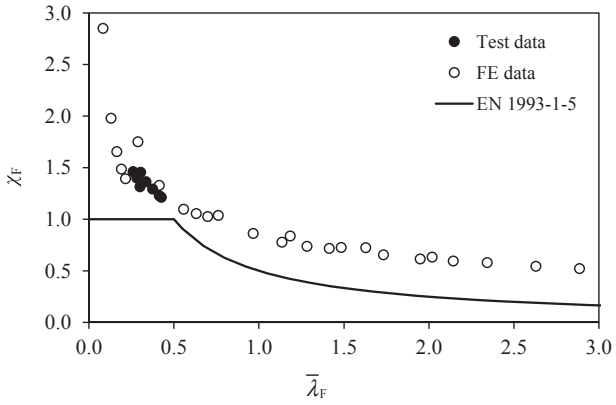

Fig. 39. Comparison of ultimate strengths determined from ITF loading tests and FE simulations against EN 1993-1-5 design curve.

4.2. North American design provisions: AISC design guide 27

The AISC Design Guide 27 [40] for the design of stainless steel hot-rolled/welded I-section members under concentrated loading refers to the carbon steel design provisions set out in ANSI/AISC 360-16 [53]. The design resistance is obtained through the evaluation of the following limit states: (i) web yielding, (ii) web crippling, and (iii) web buckling (for the internal two-flange loading only). The design equations for each limit state are set out in Table 6. No explicit rules for the interaction between concentrated transverse loading and bending moment are given [54], hence the provisions are evaluated by comparing the experimental and numerical failure loads F_u with the design resistance $F_{u,AISC}$ taken as the minimum of the values determined for the aforementioned limit states. For the IOF loading case, Table 7 shows a mean value of 2.42 for $F_u/F_{u,AISC}$ with a coefficient of variation (COV) of 0.44 for all the studied cases. Higher ratios of $F_u/F_{u,AISC}$ for stockier cross-sections are observed in Table 7 and Fig. 36, ranging from $F_u/F_{u,AISC} = 1.63$ for $h_w/t_w = 120$ to $F_u/F_{u,AISC} = 3.04$ for $h_w/t_w = 10$. For the ITF loading case, Table 8 and Fig. 38 show not only high $F_u/F_{u,AISC}$ ratios for the stockier sections (i.e. $F_u/F_{u,AISC} = 2.35$ for $h_w/t_w = 30$ to $F_u/F_{u,AISC} = 2.82$ for $h_w/t_w = 10$) but also increasing $F_u/F_{u,AISC}$ ratios for the more slender sections (i.e. $F_u/F_{u,AISC} = 2.35$ for $h_w/t_w = 30$ to $F_u/F_{u,AISC} = 7.69$ for $h_w/t_w = 120$). The former is attributed to the neglect of the strain hardening experienced by stainless steel members with stocky webs, while the latter is due to the conservatism of the web buckling limit state formulae given in AISC 360-16, which do not consider the bearing length and were only calibrated for sections with $h_w/t_w \leq 40$ [55]. This conservatism has also been observed by Menkulasi et al. [56].

5. Discussion

Overall, the evaluations presented in Sections 4.1 and 4.2 reveal that the current European and North American design provisions for stainless steel members under concentrated transverse loading are safe-sided but generally overly-conservative; this is the case for both internal one-flange (IOF) loading and internal two-flange (ITF) loading. In the low slenderness range, the under-predictions of resistance are attributed to strain hardening, which is particularly prominent in stainless steels, especially the austenitic grades. In the high slenderness range,

substantial under-predictions of resistance arose from the application of the North American design provisions to the case of ITF loading where web buckling is dominant. There is considered to be scope for the development of improved design formulae for resistance to concentrated loading that take account of the particular characteristics of stainless steel over the full slenderness range.

6. Conclusions

An extensive experimental and numerical investigation into the structural response of welded stainless steel I-beams under two types of concentrated transverse loading: (i) internal one-flange (IOF) and (ii) internal two-flange (ITF) loading has been presented. The physical experimental programme comprised twenty-four member tests: sixteen IOF tests and eight ITF tests. The experimental results were complemented by numerically generated data, allowing further investigation of the influence of the bearing length and the web slenderness on the ultimate web bearing resistance of stainless steel I-beams. Both the numerical and test results were used to assess the accuracy of the European and North American design provisions for the ultimate web bearing resistance of welded stainless steel I-sections. The results showed that the existing design rules generally lead to safe-sided but conservative resistance predictions for members with stocky webs under both loading conditions; this is attributed to the neglect of the significant strain hardening associated with stainless steel. Overly conservative results were also observed for cross-sections with slender webs. The findings of this study highlight the need for the development of new design rules for stainless steel beams under concentrated transverse loading that recognise the particular characteristics of stainless steel; this is the focus of ongoing work.

Acknowledgments

The authors would like to thank Montanstahl AG for providing the test specimens for the project. The contribution of Gordon Herbert, Les Clark and Behnam Behzadi Sofiani in the experimental part of this work, as well as the financial support of the Brazilian National Council for Scientific and Technological Development (CNPq, Brazil), are also gratefully acknowledged.

References

[1] Graham JD, Sherbourne AN, Kabbaz RN, Jensen CD. Welded interior beam-to-column connections. Am Inst Steel Constr (AISC) 1959.
[2] Granath P, Lagerqvist O. Behaviour of girder webs subjected to patch loading. J Constr Steel Res 1999;50(1):49–69.
[3] Chacón R, Herrera J, Fargier-Gabaldon L. Improved design of transversally stiffened steel plate girders subjected to patch loading. Eng Struct 2017;150(1):774–85.
[4] Macdonald M, Heiyantuduwa MA, Harrison DK, Bailey R, Rhodes J. Literature review of web crippling behaviour. In: 2nd Scottish Conference for Postgraduate Researchers of the Built and Natural Environment (PRoBE 2005), Rotterdam (Netherlands): In-house Publishing; 2005.
[5] Mijušković O, Branislav Ć, Šćepanović B, Žugić L. Analytical model for buckling analysis of the plates under patch and concentrated loads. Thin-Walled Struct 2016;101:26–42.
[6] Bakker MCM. Yield line analysis of post-collapse behaviour of thin-walled steel members. Heron 1990;35(3).
[7] Natário P, Silvestre N, Camotim D. Localized web buckling analysis of beams subjected to concentrated loads using GBT. Thin-Wall Struct 2012;61:27–41.
[8] dos Santos GB, Gardner L, Kucukler M. A method for the numerical derivation of plastic collapse loads. Thin-Walled Struct 2018;124:258–77.
[9] Winter G, Pian RHJ. Crushing strength of thin steel webs. Engineering Experiment Station, Bulletin No 35 (Part 1); 1946. p. 1–24.
[10] Yu WW, Hetrakul N. Webs for cold formed steel flexural members structural behavior of beam webs subjected to web crippling and a combination of web crippling and bending. University of Missouri-Rolla; 1978.
[11] Wing BA, Schuster RM. Web crippling of multi-web deck sections subjected to interior one flange loading. In: Eighth international speciality conference on cold-formed steel structures: recent research and developments in cold-formed steel design and construction, St Louis (MO, USA): Univ of Missouri-Rolla; 1986.
[12] Beshara B, Schuster RM. Web crippling data and calibrations of cold-formed steel members. Research Report RP00-2. University of Waterloo; 2000.
[13] Young B, Hancock GJ. Design of cold-formed channels subjected to web crippling. J Struct Eng ASCE 2001;127(10):1137–44.
[14] Young B, Hancock GJ. Cold-formed steel channels subjected to concentrated bearing load. J Struct Eng ASCE 2003;129(8):1003–10.
[15] Bhakta BH, LaBoube RA, Yu WW. The effect of flange restraint on web crippling strength. Civil Engineering Study 92-1, University of Missouri-Rolla; 1992.
[16] Cain DE, LaBoube RA, Yu WW. The effect of flange restraint on web crippling strength of cold-formed steel Z- and I- sections. Civil Engineering Study 95–2. University of Missouri-Rolla; 1995. p. 95–102.
[17] Young B, Hancock GJ. Web crippling of cold-formed unlipped channels with flanges restrained. Thin-Walled Struct 2004;42(6):911–30.
[18] Janarthanan B, Mahendran M, Gunalan S. Bearing capacity of cold-formed unlipped channels with restrained flanges under EOF and IOF load cases. Steel Constr 2015;8(3):146–54.
[19] Sivakumaran KS, Zielonka KM. Web crippling strength of thin-walled steel members with web opening. Thin-Walled Struct 1989;8(4):295–319.
[20] Uzzaman A, Lim JBP, Nash D, Rhodes J, Young B. Cold-formed steel sections with web openings subjected to web crippling under two-flange loading conditions – Part I: Tests and finite element analysis. Thin-Walled Struct 2012;56:38–48.
[21] Lian Y, Uzzaman A, Lim JBP, Abdelal G, Nash D, Young B. Web crippling behaviour of cold-formed steel channel sections with web holes subjected to interior-one-flange loading condition – Part I: Experimental and numerical investigation. Thin-Wall Struct 2017;111:103–12.
[22] Korvink SA, van der Berg GJ, van der Merwe P. Web crippling of stainless steel cold-formed beams. J Constr Steel Res 1995;34:225–48.
[23] Zhou F, Young B. Experimental and numerical investigations of cold-formed stainless steel tubular sections subjected to concentrated bearing load. J Constr Steel Res 2007;63(11):1452–66.
[24] Talja A, Hradil P. Structural Applications of Ferritic Stainless Steels (SAFSS) WP2: Structural performance of steel members – Model calibration tests. Report of the SAFSS Project – Structural Applications of Ferritic Stainless Steels, VTT-R-06130-12, VTT Technical Research Centre of Finland; 2012.
[25] Li H-T, Young B. Cold-formed ferritic stainless steel tubular structural members subjected to concentrated bearing loads. Eng Struct 2017;145:392–405.
[26] Bock M, Arrayago I, Real E, Mirambell E. Study of web crippling in ferritic stainless steel cold formed sections. Thin-Walled Struct 2013;69:29–44.
[27] Bock M, Real E. Strength curves for web crippling design of cold-formed stainless steel hat sections. Thin-Walled Struct 2014;85:93–105.
[28] Yousefi AM, Lim JBP, Uzzaman A, Clifton GC. Numerical study of web crippling strength in cold-formed austenitic stainless steel lipped channels with web openings subjected to interior-two-flange loading. In: 11th Pacific Structural Steel Conference, Shanghai; 2016.
[29] Granholm CA. Provning av balkar med extremt tunt liv (Testing of girders with extremely thin web, in Swedish). Report 202, Institutionen for Byggnadsteknik; 1960.
[30] Bergfelt A. Studies and tests on slender plate girders without stiffeners – shear strength and local web crippling. In: IABSE Colloquium on Design of Plate and Box Girders for Ultimate Strength, Lisbon, Portugal; 1971.
[31] Roberts TM, Markovic N. Stocky plate girders subjected to edge loading. Proc Inst Civil Eng, Part 2 1983;75:539–50.
[32] Dubas P, Tschamper H. Stabilite des ames soumises a une charge concentree et a une flexion globale (Stability of beams subjected to concentrated loads and bending moments, in French). Constr Metallique 1990;2:25–39.
[33] Gozzi J. Patch loading resistance of plated girders – ultimate and serviceability limit state. Department of Civil, Mining and Environmental Engineering, Lulea University of Technology, PhD thesis; 2007.
[34] Chen Y, Chen X, Wang C. Experimental and finite element analysis research on I-beam under web crippling. Mater Struct 2016;49(1–2):421–37.
[35] Zoetemeijer P. The influence of normal-, bending- and shear stresses on the ultimate compression force exerted laterally to European rolled sections. Report 6-80-5, TU Delft; 1980.
[36] Oxford J, Gauger HU. Beultraglast von Vollwandträgern unter Einzellasten (Ultimate buckling load of web girders under single loads, in German). Stahlbau 1989;58(11):331–9.
[37] Lagerqvist O. Patch loading – resistance of steel girders to concentrated forces. Division of Steel Structures, Lulea University of Technology, PhD thesis; 1995.
[38] Sélen E. Work package 3.5 – Final Report – Web crippling. Report to the ECSC Project – Development of the use of stainless steel in construction. Contract no. 7210-SA/903, Lulea University of Technology; 2000.
[39] EN 1993-1-5:2006. Eurocode 3: Design of steel structures – Part 1-5: Plated structural elements. European Committee for Standardization (CEN), Brussels; 2006.
[40] AISC Steel Design Guide 27. Structural Stainless Steel. American Institute of Steel Construction, USA; 2013.
[41] EN ISO 13919-1. Welding - Electron and laser beam welded joints – Guidance on quality levels for imperfections - Part 1: Steel. European Committee for Standardization (CEN), Brussels; 1997.
[42] Gardner L, Bu Y, Theofanous M. Laser-welded stainless steel I-sections: Residual stress measurements and columns buckling tests. Eng Struct 2016;127:536–48.
[43] EN ISO 6892-1:2009. Metallic materials - Tensile testing - Part 1: Method of test at ambient temperature. European Committee for Standardization (CEN), Brussels; 2009.
[44] Schafer BW, Pekoz T. Computational modeling of cold-formed steel: characterizing geometric imperfections and residual stresses. J Constr Steel Res 1998;47:193–210.
[45] Zhao O, Gardner L, Young B. Structural performance of stainless steel circular hollow sections under combined axial load and bending – Part 1: Experiments and numerical modelling. Thin-Walled Struct 2016;101:231–9.
[46] DaVis. Product-Manual DaVis 8.4. LaVision [Software]; 2016.
[47] ABAQUS. Abaqus version 6.14. SIMULIA - Dassault Systèmes [Software]; 2014.
[48] Bu Y, Gardner L. Finite element modelling and design of welded stainless steel I-section columns. J Constr Steel Res 2018. https://doi.org/10.1016/j.jcsr.2018.03.026. [in press].
[49] Saliba N, Gardner L. Cross-section stability of lean duplex stainless steel welded I-

sections. J Constr Steel Res 2013;80:1–14.
[50] EN 1993-1-4:2006 + A1:2015. Eurocode 3: Design of steel structures – Part 1.4: General rules - Supplementary rules for stainless steels. European Committee for Standardization (CEN), Brussels; 2006.
[51] Roberts TM, Rockey KC. A mechanism solution for predicting the collapse loads of slender plate girders when subjected to in-plane patch loading. Proc Inst Civil Eng, Part 2 1979;67:155–75.
[52] Afshan S, Gardner L. The continuous strength method for structural stainless steel design. Thin-Walled Struct 2013;68:42–9.
[53] ANSI/AISC 360-16. Specification for structural steel buildings, EUA; 2016.
[54] Ziemian RD. Guide to stability design criteria for metal structures. 6th ed. USA: Wiley; 2010.
[55] Chen WF, Newlin DE. Column web strength in steel beam-to-column connections. In: ASCE Annual and National Environmental Engineering Meeting, Missouri, USA; 1971.
[56] Menkulasi F, Farzana N, Moen CD, Eatherton MR. Revisiting web compression buckling for wide flange sections. In: Annual Stability Conference, Florida, USA; 2016.